

Flapping Flyers in Formation: Modelling Flow-Mediated Collective Flight

A Case Study in Mathematical Modelling and Scientific Computing

George Hildick-Smith

Supervised by Dr. Christiana Mavroyiakoumou

May 18, 2026

© 2026 George Hildick-Smith. This work is licensed under CC BY-NC-ND 4.0, https://creativecommons.org/licenses/by-nc-nd/4.0/. Third party images and quotations remain the property of their owners.

1 Introduction



Figure 1: *A flock of birds flying in a line formation, source*[1].

In this report, we are motivated by birds, specifically how and why they fly in formations as seen in Figure 1. Initially, we might think that a lot of this behaviour comes from social interactions between birds, such as safety in numbers or improved communication and resource sharing among each other. While these may be true, we see in [1] that model foils mechanically flapped in a fluid exhibit very similar flocking behaviour to birds, while only interacting through fluid dynamics. This suggests that the fluid dynamics may be a main driving factor of this behaviour. We explore this idea by modelling what we call *flyers* (which could represent birds, fish, or even drones) moving in a fluid.

To study this, we follow [2] and reduce the problem to a one-dimensional chain of flyers coupled through a simple wake model. In this model, each flyer's horizontal motion is governed by thrust due to its flap and the wake it experiences, and drag due to motion in the fluid. Despite this simplicity, the model captures the essential physics, including the delayed coupling of adjacent flyers and the decay of the wake.

We begin with a single flyer to establish a baseline of how the model works, so we can better understand the system's behaviour as we introduce extensions such as a constant background wake or multiple flyers. After forming these models, we use them to explore questions about the stability of different flapping formations. We look at whether different formations are stable to small perturbations or if the flyers will separate or collide given the setup. This gives us some intuition into what kind of formations we might expect to see in nature. For example, it has been shown that the average heart rate of pelicans flying in formation can be reduced by up to 14% [3], confirming that the spacing choices made by a formation can have substantial benefits. The final section investigates what an optimal formation might look like. We define a measure for the energy expended and compare greedy (each flyer minimises for themselves) and cooperative (the formation minimises for the group) strategies. This could, for example, inform the design of drone arrangements for energy efficiency.

[1] https://tinyurl.com/bdd86e3m

2 Model Formulation

We wish to create a model that exhibits the essential interactions between flyers mediated by the fluid, while being simple enough to be analytically tractable and admit efficient numerical simulation. Hence, we follow the approach of Mavroyiakoumou in [2] throughout this section and reduce the problem to one dimension in space. We also model the flyers as thin foils that only move vertically and do not pitch or roll. We consider a chain of N thin flyers in single-file, each capable of prescribed vertical oscillation that we may refer to as a *flap*. For the n^{th} flyer at time t, we let

- $X_n(t)$ and $Y_n(t)$ denote the **horizontal and vertical positions** of the flyer,
- $V_n(t)$ denote the prescribed **vertical flapping velocity** of the flyer,
- $B_n(t)$ denote the **resultant vertical velocity** of the flyer,
- $U_n(t) = \dot{X}_n$ denote the **resultant horizontal velocity** of the flyer,
- $W_n(x,t)$ denote the **vertical velocity of the wake** shed by flyer n at x,

where $n = 1$ is the leader and $n = 2, \ldots, N$ are the followers. Note that as the flyers are single-file, $X_1 > \cdots > X_N$. We now consider the active forces shown in Figure 2.

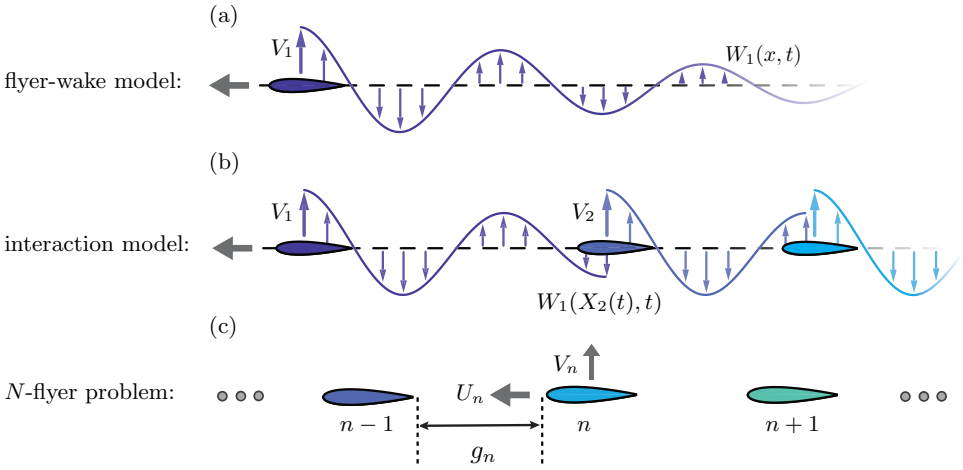


Figure 2: ***(a)*** *The leading flyer generates a wake that decays downstream.* ***(b)*** *A follower at position $X_2(t)$ experiences the wake velocity $W_1(X_2(t))$.* ***(c)*** *The gap $g_n = X_{n-1}(t) - X_n(t) - c$ between adjacent flyers. This diagram from [2].*

Each flyer is assigned a prescribed vertical flapping velocity; for the majority of this report, we use the simplest and most natural form,

$$Y_n(t) = A_n \sin(2\pi f_n t), \quad \text{so} \quad V_n(t) = \pi A_n f_n \cos(2\pi f_n t), \tag{1}$$

which mimics the sinusoidal flapping seen in birds and is illustrated by the wake in Figure 2. Here A_n is the flapping amplitude (peak to trough) and f_n is the frequency of flyer n.

2.1 The Drag Law

The flyer moves horizontally through the viscous fluid, so it experiences a drag force opposing its motion. We model this as viscous skin friction,

$$D_n = \frac{C_D s\sqrt{\rho\mu c}}{2}\, U_n^{3/2}, \tag{2}$$

where μ is the dynamic viscosity and C_D is the non-dimensional drag coefficient. The $U_n^{3/2}$ scaling arises from boundary-layer theory for a flat plate in laminar flow [2].

2.2 The Thrust Law

As each flyer flaps, it accelerates the surrounding fluid, and the reaction force on the wing has a component in the horizontal direction. This is the thrust. In this model, from potential flow theory for a thin foil in an incompressible fluid, we get

$$T_n = \frac{\rho C_T c s}{2}\, B_n^2, \tag{3}$$

where ρ is the fluid density, c is the chord length (vertical width), s is the wing span, and C_T is the non-dimensional thrust coefficient.

2.3 The Wake Model

To evaluate the thrust in Equation (3), we need to know B_n. This is the difference between the prescribed flapping velocity V_n and the vertical velocity of the wake shed by the preceding flyer, W_{n-1}, at the current position of flyer n. Hence,

$$B_n(t) = V_n(t) - W_{n-1}\big(X_n(t), t\big). \tag{4}$$

This uses an assumption called *erase-and-replace*, which means that the wake felt is solely due to the flyer ahead. In reality, the superposition of wakes from all flyers ahead would be felt, but the added complexity is not justified by the marginal improvement in accuracy. Since flyer $n-1$ is always ahead, it passed through position $X_n(t)$ at some earlier moment given by $t - t_n(t)$. We call $t_n(t)$ the *delayed time*, defined implicitly by

$$X_n(t) = X_{n-1}\big(t_n(t)\big). \tag{5}$$

As flyer n advances, t and $t_n(t)$ increase monotonically, tracking further forward through the history of flyer $n-1$. The wake decays exponentially with the time elapsed since it was generated, so the wake velocity at $X_n(t)$ is

$$W_{n-1}\big(X_n(t), t\big) = V_{n-1}\big(t_n(t)\big)\, e^{-(t-t_n(t))/\tau}, \tag{6}$$

where $\tau > 0$ is the wake decay timescale [1]; larger τ means a more persistent wake and stronger inter-flyer coupling. For the leader, the surrounding fluid is quiescent[2], so $W_0 \equiv 0$ and $B_1 = V_1$.

[2]Quiescent: at rest, with no background flow or wake.

2.4 Equations of Motion

Bringing together Equations (2) and (3), we apply Newton's second law in the horizontal direction, with all flyers assumed to have equal and constant mass M,

$$\dot{U}_n = \frac{1}{M}(T_n - D_n), \qquad n = 1, \ldots, N. \tag{7}$$

Substituting Equations (2), (3) and (6) into Equation (7), the full system of delay differential equations (DDEs) is

$$\dot{X}_n = U_n, \tag{8}$$

$$\dot{U}_n = \frac{\rho C_T c s}{2M}\left[V_n(t) - V_{n-1}(t_n)e^{-(t-t_n)/\tau}\right]^2 - \frac{C_D s\sqrt{\rho\mu c}}{2M}\,U_n^{3/2}, \tag{9}$$

$$\dot{t}_n = \frac{U_n(t)}{U_{n-1}(t_n)}, \tag{10}$$

for $n = 1, \ldots, N$, with $n = 1$ uncoupled (no V_0 term) and $t_1 \equiv t$. Equation (10) is derived by differentiating Equation (5) with respect to t. To close the system, we must specify initial conditions $X_n(0)$, $U_n(0)$, and $t_n(0)$ for each flyer, where $t_n(0)$ is determined implicitly by the initial positions via $X_n(0) = X_{n-1}(t_n(0))$.

2.5 Schematic of Configurations

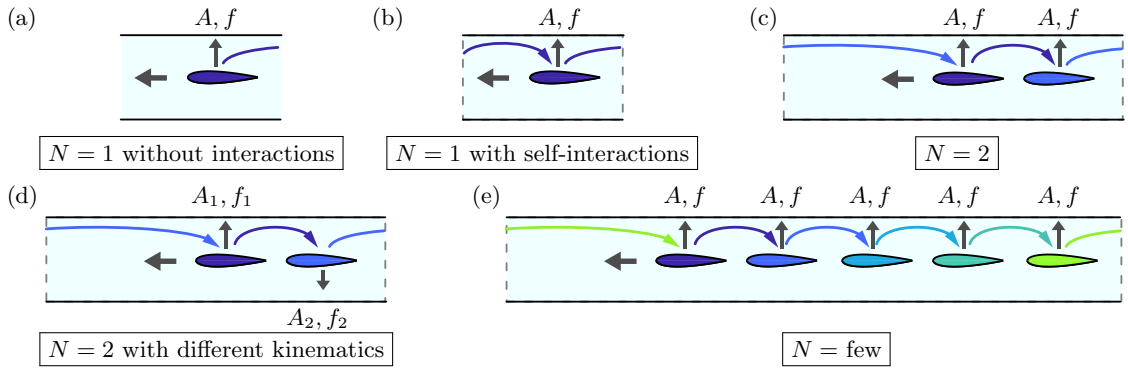


Figure 3: *Schematic of the possible configurations considered, adapted from [2].* ***(a)*** *$N = 1$ without interactions: a single free flyer in quiescent fluid, establishing the baseline.* ***(b)*** *$N = 1$ with self-interactions: a single flyer that re-encounters its own wake.* ***(c)*** *$N = 2$ with self-interactions: flapping with identical amplitudes and frequencies.* ***(d)*** *$N = 2$ with self-interactions: flapping with distinct amplitudes and frequencies.* ***(e)*** *N few flyers: a short open-loop chain, to analyse collective behaviour. In all cases, except* ***(a)****, the closed configuration is represented by cyclic boundary conditions.*

3 Non-dimensionalisation

There are five relevant physical and kinematic quantities associated with each flyer: chord length c [cm], span s [cm], mass M [g], flapping amplitude A [cm], and flapping frequency f [s^{-1}], together with the two fluid properties, density ρ [$\mathrm{g\,cm}^{-3}$] and dynamic viscosity μ [$\mathrm{g\,cm}^{-1}\,\mathrm{s}^{-1}$], and finally the wake decay timescale τ [s]. We non-dimensionalise Equations (8) to (10) by the flapping amplitude A and the characteristic timescale $1/f$. Using tildes to denote dimensionless quantities, let

$$\tilde{t} = ft, \qquad \tilde{X}_n = \frac{X_n}{A}, \qquad \text{and} \qquad \tilde{U}_n = \frac{U_n}{Af}. \tag{11}$$

The dimensionless versions of Equation (8) and Equation (10) are in the same form as before. Substituting Equations (1) and (11) into Equation (9) and rearranging gives Equation (13) in the system of DDEs for $n = 2, \ldots, N$:

$$\dot{\tilde{X}}_n(\tilde{t}) = \tilde{U}_n(\tilde{t}), \tag{12}$$

$$\dot{\tilde{U}}_n(\tilde{t}) = \gamma_T \Big[\cos(2\pi\tilde{t}) - \cos\big(2\pi\tilde{t}_n(\tilde{t})\big)\, e^{-(\tilde{t}-\tilde{t}_n(\tilde{t}))/\tilde{\tau}}\Big]^2 - \gamma_D\, \tilde{U}_n^{3/2}(\tilde{t}), \tag{13}$$

$$\dot{\tilde{t}}_n(\tilde{t}) = \frac{\tilde{U}_n(\tilde{t})}{\tilde{U}_{n-1}\big(\tilde{t}_n(\tilde{t})\big)}. \tag{14}$$

The leader has no wake interaction term, so Equation (13) reduces to

$$\dot{\tilde{U}}_1(\tilde{t}) = \gamma_T \cos^2(2\pi\tilde{t}) - \gamma_D\, \tilde{U}_1^{3/2}(\tilde{t}). \tag{15}$$

Here, the thrust and drag prefactors are

$$\gamma_T = \frac{C_T \pi^2 A^*}{2M^*}, \qquad \gamma_D = \frac{C_D A^*}{2M^* \sqrt{\mathrm{Re}_f}}, \tag{16}$$

using the five independent dimensionless parameters,

$$M^* = \frac{M}{\rho c^2 s}, \quad \mathrm{Re}_f = \frac{\rho A f c}{\mu}, \quad A^* = \frac{A}{c}, \quad s^* = \frac{s}{c}, \quad \text{and} \quad \chi = f\tau. \tag{17}$$

Here M^* is the dimensionless mass, Re_f is the flapping Reynolds number, A^* is the dimensionless amplitude, s^* is the planform aspect ratio (which does not appear explicitly in the system), and χ is the dimensionless wake decay timescale. γ_T sets the scale of the thrust and grows with dimensionless amplitude A^*; γ_D sets the scale of the drag and decreases with faster flapping (higher Re_f). Parameter values can be found in Appendix A. In later numerical simulations, we follow [2] and work with a single combined parameter such that Equation (20) simplifies. To this end, we choose

$$\gamma = \gamma_D, \qquad \text{and} \qquad \gamma_T = 2\gamma. \tag{18}$$

To keep notation simple, we now drop the tildes.

4 Single-Flyer

We begin with the simplest case, a single isolated flyer with no self-interactions, corresponding to configuration **(a)** in Figure 3. This serves as a baseline simulation in the simplest setting, so we may gain meaningful insights when we alter the system.

4.1 Steady-State Speed

With no self-interactions, we get Equation (15), which we now write as

$$\dot{U} = \gamma_T V^2 - \gamma_D U^{3/2}, \tag{19}$$

where $V(t) = \pi \cos(2\pi t)$ is the dimensionless flapping velocity (with A and f absorbed into the velocity scale Af). A steady state requires $\dot{U} = 0$, which is equivalent to $\gamma_T V^2 = \gamma_D U^{3/2}$. Since V is periodic, we integrate to find the average speed U^*,

$$U^* = \left[\frac{\gamma_T}{\gamma_D}\int_0^1 V(t)^2\,dt\right]^{2/3} = \left[\frac{\gamma_T}{\gamma_D}\,\pi^2\langle\cos^2(2\pi t)\rangle\right]^{2/3} = \pi^{4/3}\left[\frac{2\gamma_T}{\gamma_D}\right]^{2/3}. \tag{20}$$

In dimensional form, restoring the scales $U \to Af \cdot U$ and accounting for γ_T and γ_D,

$$U^*(A,f) = \left(\frac{\rho c}{\mu}\right)^{1/3}\left(\frac{C_T}{2C_D}\right)^{2/3}(\pi A f)^{4/3}, \tag{21}$$

this power law arises from Blasius skin-friction drag ($D \propto U^{3/2}$) used in Equation (2) from [4] and distinguishes this model from earlier quadratic-drag treatments [1], [5].

4.2 Numerical Results

To verify our theory, we simulate the original dimensional ordinary differential equations (ODEs) Equations (8) and (9) to recover the $(Af)^{4/3}$ scaling derived. Since the leader has no predecessor, $W_0 \equiv 0$ and $B_1 = V_1$. Dropping subscripts, Equation (9) reduces to

$$\dot{U} = \frac{\rho C_T c s}{2M}\,V(t)^2 - \frac{C_D s\sqrt{\rho\mu c}}{2M}\,U^{3/2}, \tag{22}$$

with flapping velocity $V(t) = \pi A f \cos(2\pi f t)$. We take initial conditions $X(0) = 0$ and $U(0) = U^*(A,f)$ from Equation (21), so the system starts near its predicted average velocity and the transient is short.

To interpret the results of the simulations, we use three dimensionless quantities. Firstly, the *forward Reynolds number* $Re = \rho U c/\mu$ measures the ratio of inertial to viscous forces, indicating the flow regime (laminar or turbulent). Then the *flapping Reynolds number* $Re_f = \rho A f c/\mu$ plays the same role but based on the flapping speed Af, hence is set by the parameters of the system. Note that from Equation (21), we expect $Re \propto Re_f^{4/3}$. Finally, the *Strouhal number* $St = fA/U^*$ is the ratio of flapping speed to forward speed, and is a good predictor of propulsive efficiency, with biological swimmers and flyers tending to operate in the range $St \in (0.2, 0.4)$ [6], [7].

The results of the simulations are shown in Figure 4. The agreement of the theory and simulation in panel **(a)** confirms that the system reaches a well-defined average velocity consistent with Equation (21). Substituting Equation (21) into $St = fA/U^*$ gives $St \propto (Af)^{-1/3}$, so St decreases weakly with flapping intensity. In panels **(b)** and **(c)** we observe the expected scalings $Re \propto Re_f^{4/3}$ and $St \propto Re_f^{-1/3}$.

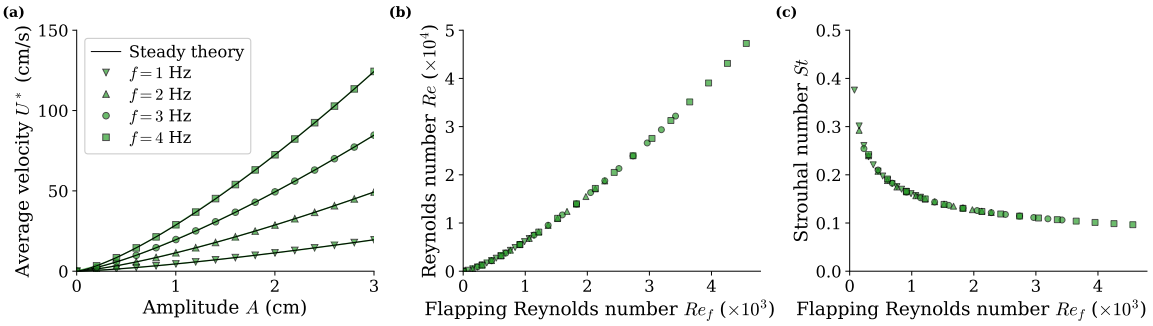


Figure 4: ***(a)*** *Time-averaged steady-state velocity U^* vs. flapping amplitude A for $f \in \{1, 2, 3, 4\}$ Hz; solid black curves show the analytical prediction Equation (21).* ***(b)*** *Forward Reynolds number Re vs. flapping Reynolds number Re_f; showing $Re \propto Re_f^{4/3}$.* ***(c)*** *Strouhal number St vs. Re_f; as $Re_f \propto Af$, then $St \propto Re_f^{-1/3}$.*

The single-flyer simulation is shown in Appendix B, with an animation of the flyer[3].

4.3 Constant Background Wake

Before tackling the full multi-flyer DDE system, we isolate the effect of constant wake, so later we can better appreciate the impact of wake interactions. We therefore consider a single flyer with a constant background wake of amplitude W — imagine a constant updraft of wind. This admits a clean analytical solution, giving intuition for how wake strength affects the average velocity. The dimensionless ODE becomes

$$\dot{U} = \gamma_T (V(t) - W)^2 - \gamma_D U^{3/2}. \tag{23}$$

The background wake changes the resultant vertical velocity $B(t)$ from $V(t)$ to $V(t) - W$. At steady state $\gamma_D {U_W^*}^{3/2} = \gamma_T \langle (V - W)^2 \rangle$, so

$$U_W^* = \left[\frac{\gamma_T}{\gamma_D} \left\langle (V - W)^2 \right\rangle \right]^{2/3} = \left[\frac{\gamma_T}{\gamma_D} \left(\frac{\pi^2}{2} + W^2 \right) \right]^{2/3}, \tag{24}$$

For $W = 0$ this recovers Equation (20). Crucially, $U_W^* > U^*$ for all $W \neq 0$ — the background wake always increases the average velocity. This is perhaps counterintuitive; one might expect a constant wake to impede flight, but the quadratic thrust law from Equation (3) means that any non-zero relative velocity, even one opposing the flap, contributes positively to thrust on average.

[3] https://youtu.be/3KM2X9eWMZM

We simulate the dimensional version of Equation (23), showing the results in Figure 5. In **(a)**, we show the prescribed velocity V from Y in Equation (1) having amplitude $A = 10\,\text{cm}$, frequency $f = 1\,\text{Hz}$. On top of this is the background wake $W = 2\pi\,\text{cm/s}$. We indicate when the flyer is in up-stroke with the light green bands and down-stroke with the light red bands. In **(b)**, we show the forward velocity $U(t)$ which oscillates around U_W^*, but we also see some other interesting behaviour. In the down-strokes, we see huge acceleration, nearly tripling the velocity. Conversely, in **(c)**, where we show the path of the flyer in the co-moving frame $X - U_W^*$, during the up-strokes the flyer is moving backwards and hence decelerating. This is because the flyer gets a boost when it flaps downwards into the wake, as it effectively moves much more air and hence generates more thrust. In the up-strokes, the converse happens, and it moves relatively little air, meaning it generates less thrust. We provide an animation of Figure 5 here[4].

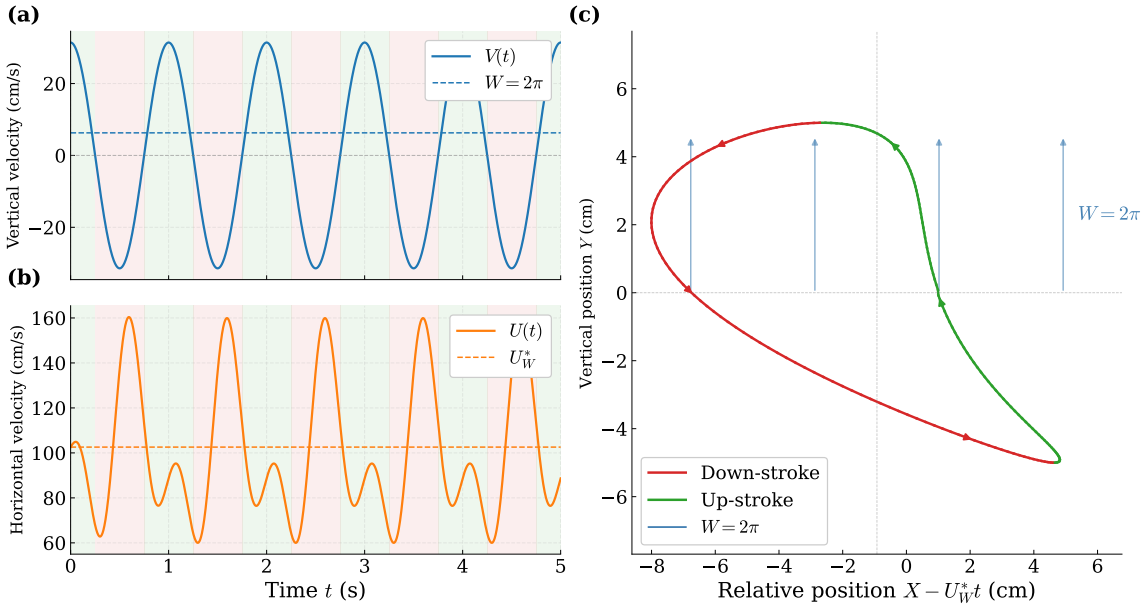


Figure 5: ***(a)*** *Flapping velocity $V(t)$ with background wake $W = 2\pi$ cm/s (dashed); green/red bands mark up-/down-strokes.* ***(b)*** *Forward velocity $U(t)$ oscillating about U_W^* (dashed).* ***(c)*** *Resultant path in the horizontally co-moving frame $X - U_W^* t$.*

As W increases, the loop traced in the co-moving frame narrows. The up- and down-stroke arcs flatten toward one another until the orbit degenerates into a thin band with vertices at $(-l, A/2)$ and $(l, -A/2)$, where $l \to \infty$ as $W \to \infty$. In this limit, the flyer moves a huge amount of air regardless of stroke direction. However, a down-stroke now solely accelerates the flyer, while an up-stroke only decelerates it. For negative W, the same results hold but are flipped about the X-axis of **(c)**.

[4] https://youtu.be/tSTnLAr7sNw

5 Multiple Flyers

Having established the single-flyer baseline, we now extend to a chain of N flyers in single-file, all flapping with the same prescribed velocity

$$V(t) = \pi A f \cos(2\pi f t), \tag{25}$$

from a flap Y with amplitude $A = 10\,\text{cm}$ and frequency $f = 1\,\text{Hz}$. The leader ($n = 1$) flaps into quiescent fluid, while each follower $n \geq 2$ experiences the wake of the flyer directly ahead, as described in Section 2.3. All flyers start at the equilibrium U^*.

5.1 Governing Equations

The system is governed by Equations (8) to (10) with the erase-and-replace wake model. Explicitly, for $n = 2, \ldots, N$,

$$\dot{U}_n = \gamma_T \, B_n(t)^2 - \gamma_D \, U_n^{3/2}, \qquad B_n(t) = V(t) - V(t_n(t)) \, e^{-(t - t_n(t))/\tau}, \tag{26}$$

where $t_n(t)$ is the delayed time defined implicitly by $X_{n-1}(t_n(t)) = X_n(t)$, and γ_T, γ_D are the dimensionless thrust and drag coefficients defined in Equation (16). The leader satisfies the same equation with $B_1 = V(t)$. The initial positions, $X_i(0)$ for $i = 1, \ldots, N$, play a significant role in the resultant dynamics of the system. This is made evident in Figure 6, where the limiting state of the second and third flyers is different in each case. These differences arise when the wake generated by the flyer in front has decayed enough to no longer support the follower, and hence it falls behind.

5.2 Numerical Results

We solve the system sequentially. We first solve the leader's ODE for $X_1(t)$, then, as this is a monotonic (strictly increasing) function in time, we can invert it. Hence, $X_1(t_1(t)) = X_2(t)$ can be rearranged to $t_1(t) = X_1^{-1}(X_2(t))$. This can be substituted into Equation (26) for $n = 2$ to solve for $X_2(t)$ and $U_2(t)$. This trick can be repeated for each follower. We used `scipy.integrate.solve_ivp` to solve the ODEs, and `scipy.interpolate.interp1d` to perform the inversion of the trajectories in Python.

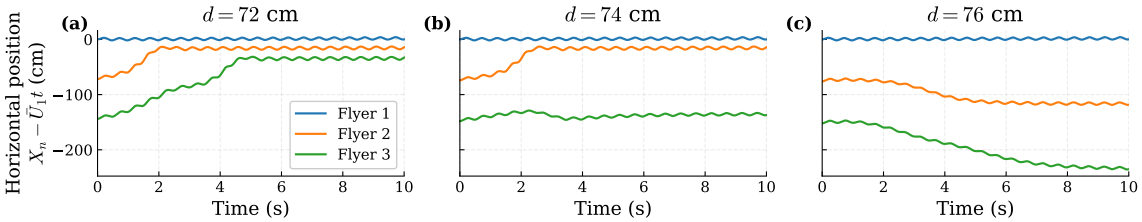


Figure 6: *Horizontal positions relative to the average speed of the leader over time. We use initial separations of* $[72, 74, 76]$ *cm. Animations of (a), (b) and (c) are provided* [5].

[5] **(a)** — https://youtu.be/msMGbctblI4, **(b)** — https://youtu.be/hBRKF8ehYFE, **(c)** — https://youtu.be/6UvT0KvKrEU

6 Stability Analysis

The multiple-flyer results in Section 5 assumed all flyers flap with the same amplitude A and frequency f. Here, we relax this assumption and simplify to $N = 2$, then ask whether the formation remains stable if the follower flaps differently from the leader. We parameterise the two ratios as,

$$k_1 = \frac{A_2}{A_1}, \qquad k_2 = \frac{f_2}{f_1}, \tag{27}$$

where $k_1 = k_2 = 1$ corresponds to the identical-flapping baseline. For each (k_1, k_2) pair, we run a two-flyer simulation and classify the outcome as one of three events:

- **Stable** — the gap $X_1 - X_2$ remains bounded throughout $t \in [0, 100]$ s.
- **Collision** — the gap falls to zero, so the follower meets the leader at some time.
- **Separation** — the gap exceeds 300 cm, so the follower is effectively decoupled[6].

To check sensitivity to starting conditions, each (k_1, k_2) pair is tested at three initial gaps: $0.5\,d^*$, d^*, and $1.5\,d^*$, where d^* is the analytical equilibrium spacing for the follower's own flapping parameters (see Appendix C).

6.1 Parameter Setup

For a given (k_1, k_2) pair, we fix the ratios symmetrically around $\bar{A} = 10$ cm and $\bar{f} = 1$ Hz.

$$A_1 = \frac{2\bar{A}}{k_1 + 1}, \quad A_2 = \frac{2k_1\bar{A}}{k_1 + 1}, \qquad f_1 = \frac{2\bar{f}}{k_2 + 1}, \quad f_2 = \frac{2k_2\bar{f}}{k_2 + 1}. \tag{28}$$

The amplitude and frequency ratios k_1 and k_2 are swept over $[0.1, 2.0]$ in steps of 0.1.

6.2 Stability Diagram

The results are shown in Figure 7. The most immediate takeaway is that if the second flyer flaps with a smaller amplitude or lower frequency than the leader, then the formation tends to separate. Conversely, with a larger amplitude or higher frequency, we tend to a collision. The interesting results lie around the curve $k_1 k_2 = 1$.

This curve is a contour along which the follower generates the same mean thrust as the leader, passing through $(1, 1)$. It balances the mean thrust and drag for each flyer as $k_1 k_2 = 1$ implies $A_2 f_2 = A_1 f_1$ and the terminal speed is $U^* \propto (Af)^{4/3}$ from Equation (21), so the follower reaches the same terminal speed as the leader.

We therefore expect stable setups to compensate for a larger amplitude with a proportionally lower frequency (or vice versa), so that $k_1 k_2 \approx 1$. The individual cases of each initial separation and their stability, separation, and collision results are shown in Appendix D. It is from these that Figure 7 is constructed, mimicking Figure 4 of [5].

[6] This is due to the wake essentially decaying to zero at this distance.

What we find is that stable cases can exist **above** the dashed curve. If we take the example of $k_1 = 1.3$ and $k_2 = 0.9$ (indicated by the black dot in Figure 7), then the follower has a larger amplitude but lower frequency than the leader. In Figure 8 we have $k_2 \neq 1$ from two distinct frequencies, hence the system has two distinct periods. One from the leader's flapping, $T_1 = 1/f_1 \approx 0.95$s, and the other $T_2 = 1/|f_1 - f_2| \approx 9.5$s when both cycles match up again.

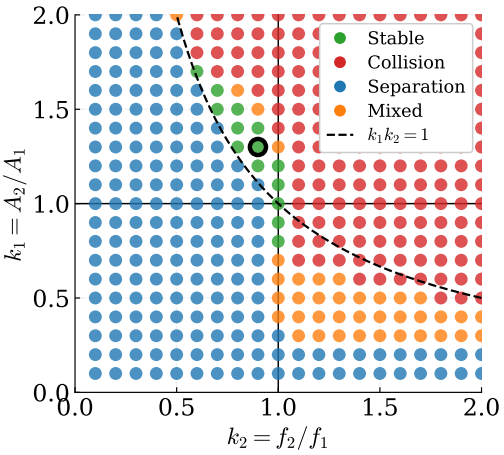


Figure 7: *Stability diagram: each point is coloured by its outcome across all three initial gaps — $[0.5d^*, d^*, 1.5d^*]$. Orange indicates a mixed outcome; otherwise the result is consistent. The black circle marks $k_1 = 1.3$, $k_2 = 0.9$ as a guide for Figure 8.*

The explanation is that the follower is initially not beneficially aligned with the leader's wake. That is, when the follower is near the leader, the wake is strong and in the same direction as the flap. This means the follower is moving less air and hence falls behind the leader. Eventually, it is far behind enough that the wake becomes aligned with its flap, and it has a few flaps of acceleration before the cycle repeats. This can be seen in the limit-cycle path traces in Figure 8 **(b)**, where the flyers trace out loops.

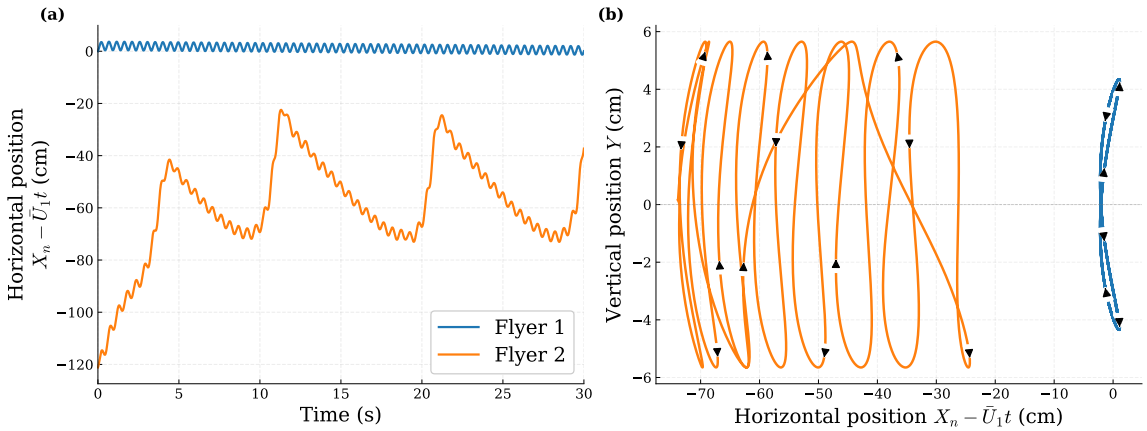


Figure 8: *Simulation with $k_1 = A_2/A_1 = 1.3$ and $k_2 = f_2/f_1 = 0.9$, initialised at $d = d^*$.* ***(a)*** *Horizontal position relative to the mean speed of the leader against time.* ***(b)*** *Limit-cycle path traces in the co-moving frame, with arrows indicating direction of travel. An instructive animation of this figure can be found here[7].*

[7] https://youtu.be/3dPvhiTY-QY

7 Constant Separation

We have now considered how a system may be stable or unstable (separations and collisions). This motivates us to ask what the *most* stable configuration is. Our answer is flyers at a constant separation[8], where each follower adapts its flap to the wake it experiences, so we solve for V_n (rather than X_n) using the non-dimensional ODEs from Equations (12) to (14) with $\gamma = 10$ and $V_1(\tilde{t}\,) = \cos(2\pi\tilde{t}\,)$, matching Figure 2(d) of [8].

The key quantity is the delay $\tilde{t}_n(\tilde{t}\,)$, defined as the time at which flyer $n-1$ occupied the current position of flyer n, i.e., $\tilde{X}_{n-1}(\tilde{t}_n) = \tilde{X}_n(\tilde{t}\,)$. Constant separation requires $\tilde{X}_n(\tilde{t}\,) = \tilde{X}_{n-1}(\tilde{t}\,) - d$, so substituting gives $\tilde{X}_{n-1}(\tilde{t}_n) = \tilde{X}_{n-1}(\tilde{t}\,) - d$. Since all flyers share the same speed profile, $\tilde{X}_{n-1} - \tilde{X}_1 = c_n$ for some constant c_n, giving $\tilde{X}_1(\tilde{t}_n) = \tilde{X}_1(\tilde{t}\,) - d$. Crucially, this is independent of n, so a single inversion of the leader trajectory yields $\tilde{t}_n$ for all $n \geq 2$. Setting $B_n = \sigma_n V_1(\tilde{t}\,)$ (matching the leader's thrust, with $\sigma_n = \pm 1$ a free choice since thrust depends on B_n^2) and solving gives

$$V_n(\tilde{t}\,) = \sigma_n V_1(\tilde{t}\,) + V_{n-1}\big(\tilde{t}_n(\tilde{t}\,)\big)\, e^{-(\tilde{t}-\tilde{t}_n(\tilde{t}))/\chi}, \tag{29}$$

where we solve for each new V_n iteratively. Recall $\chi = f\tau$ from Equation (17) is the dimensionless wake decay timescale. Figure 9 shows the result for $N = 5$. In **(a)**, the flapping velocities converge quickly — the system acts as a filter, with wake-induced distortions washing out down the chain. In **(b)**, all flyers trace figure-eights in the co-moving frame, but the leader moves forwards in the first half of each loop while the followers accelerate in the second half. An animation can be found here[9].

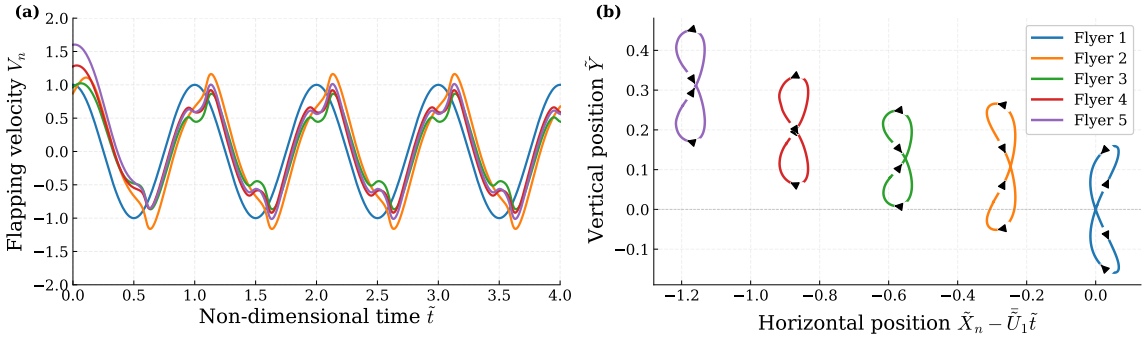


Figure 9: *Constant separation simulation ($N = 5$, $d = 0.3$, $\gamma = 10$, $\sigma_n = 1$ for all n). **(a)** Flapping velocities $V_n(\tilde{t}\,)$. **(b)** Limit-cycle path traces in the co-moving frame.*

[8] We only consider the case where the leader has a flap as given in Equation (1), although the method works for any prescribed flap. A degenerate solution would be to have all flyers stationary.

[9] https://youtu.be/7GVSroqmvN8

8 Optimal Spacing

Given the constant separation flapping formula Equation (29), a natural question is what separation d_n each follower $n \geq 2$ should maintain from its predecessor to minimise the effort put in. To answer this, we first define the effort put in as the average amplitude of the flapping velocity $V_n(\tilde{t}, d)$ that maintains a distance d,

$$E_n(d) = \int_0^1 |V_n(\tilde{t}, d)| \, d\tilde{t}. \tag{30}$$

We then normalise these by dividing by the leader's effort E_1, giving the relative effort $\hat{E}_n = E_n/E_1$. Another choice we must make besides the separation distance is whether the follower flaps in-phase ($\sigma_n = +1$) or out-of-phase ($\sigma_n = -1$) with the leader. Not every combination of (d, σ_n) is stable as we saw in Section 6. Following [8], the linearised dynamics about the fixed point yield the stability criterion

$$S(\sigma_n, d, \chi) \;=\; -\sigma_n[\cos(2\pi d) + 2\pi\chi \sin(2\pi d)] < 0, \tag{31}$$

which requires $\sigma_n A(d) > 0$, where $A(d) = \cos(2\pi d) + 2\pi\chi \sin(2\pi d)$. Intuitively, this condition ensures that small perturbations to the separation d decay rather than amplify. For a given d, the sign of $A(d)$ determines which phase choice is stable. When $A(d) > 0$ only $\sigma_n = +1$ is stable, and when $A(d) < 0$ only $\sigma_n = -1$ is stable. This can be seen in Figure 10, where only one of the blue or red curves is solid for each d.

A minimum separation $d_{\min}$ is imposed for feasibility, which allows the flyers to have some length that they occupy behind their coordinate. Setting $d_{\min} = 0.3$ ensures, from Figure 10, that the flyers are not encouraged to be as close as possible. This excluded region is marked with grey shading.

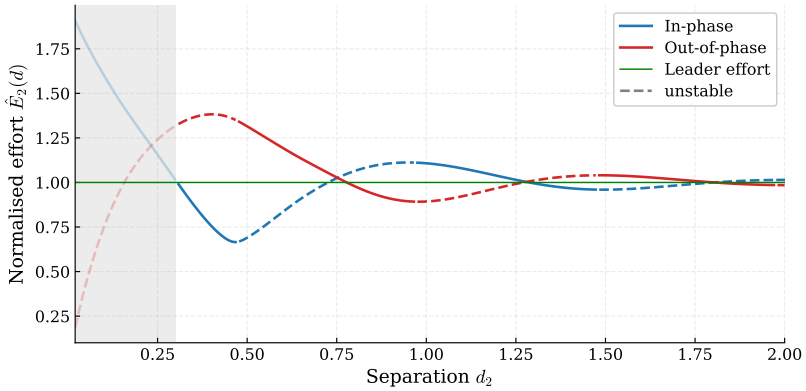


Figure 10: *Normalised flapping effort $\hat{E}_2(d_2)$ with $d_{\min} = 0.3$ for the first follower ($n = 2$). Blue and red curves correspond to the in-phase ($\sigma_n = +1$) and out-of-phase ($\sigma_n = -1$). Solid segments indicate linear stability while dashed segments are unstable from Equation (31). The shaded region is excluded as a physical collision constraint.*

We can conclude that if the effort $\hat{E}_n$ is less than one, then the follower is flapping with less effort than the leader, and hence it is beneficial for the follower to fly behind the leader. Depending on what distance the first follower settles on, the second follower will have a different optimal distance and possibly phase.

For $N \geq 3$, we employ two different strategies to find the optimal separation d_n^* and phase σ_n for each follower n. The first is a greedy strategy, where we minimise the effort for each flyer sequentially. The second is a cooperative strategy, where we minimise the average of the efforts of all followers. The results of both are shown in Figure 11.

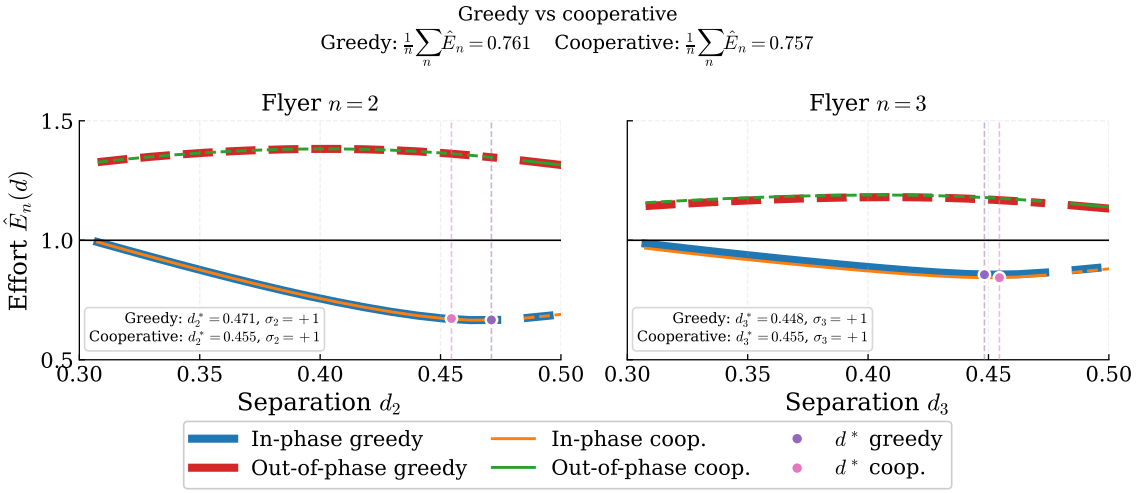


Figure 11: *Normalised flapping effort $\hat{E}_n(d)$ for each follower with ($N = 3$, $d_{\min} = 0.3$), comparing the greedy strategy (blue and red, thick) against the cooperative strategy (orange and green, thin). Solid segments are linearly stable, and dashed segments are unstable. The purple and pink markers indicate the respective optima d_n^*. This plot has been scaled for visibility from Figure 10. Full non-overlapping versions can be found in Appendix E.*

A natural explanation for the greedy approach is that each flyer tries to ride the wake generated by the flyer in front and flap with as little effort as possible. This puts it in a position of instability where a slight perturbation backwards means the wake is no longer as helpful and the flyer will separate.

For the cooperative strategy, the first follower ends up flapping slightly more than in the greedy case, but this allows it to generate more wake for the second follower, which can then flap less, and on average, less energy is used. In Figure 11, there is a 0.526% reduction in the average effort of the group compared to the greedy strategy, but a 24.3% reduction compared to each flyer acting entirely alone. This is a significant benefit, especially if applied to a bird over a long migratory flight, and reductions like this could give cooperative birds a competitive advantage.

9 Conclusion

In this report, we have developed a series of models for collective flight, building up from a single isolated flyer up to optimally spaced multi-flyer formations. At each stage we have considered both analytical tractability and physical feasibility.

Having formed the model, we begin with the simplest case, a single flyer in quiescent fluid. Equation (19) admits a clean steady-state solution Equation (21), from which the equilibrium speed scales as $U^* \propto (Af)^{4/3}$ due to Blasius drag. This shows that the model behaves as in [2], [8]. We then subject the flyer to a constant background wake W, finding that any non-zero wake always increases the average speed via the quadratic thrust law regardless of its sign or strength. This perhaps counterintuitive result foreshadows the advantage that flapping in a formation gives.

We then introduced multiple flyers and wake interactions between them in Section 5. We considered a chain of N identical flyers all flapping with the same sinusoidal profile interacting through Equation (6). The simulations in Figure 6 demonstrated that for this setup, the initial separation determined the outcomes of the simulation. This sensitivity motivated the stability analysis in Section 6, where we relaxed the identical-flapping assumption and classified simulations as stable, colliding, or separating for different initial distances, amplitudes, and frequencies. Figure 7 showed that stability occurs roughly when the follower generates the same mean thrust as the leader, captured by the curve $k_1 k_2 = 1$. We also found that stable configurations above this curve exist, which interestingly exhibited two distinct periods.

Section 7 answers what the *most* stable configuration is. Here, we flip the problem on its head and solve for the flap that maintains a constant separation between all flyers. Due to the strictly monotonically increasing position of the flyers, we form Equation (29) and iteratively solve it, converging quickly to a solution.

Bringing the problem back to reality, we look at how we should space these flyers and if they should flap in or out of phase to minimise energy expenditure. We define the normalised effort $\hat{E}_n$ as the mean absolute flapping speed required to hold a distance d_n relative to the effort of the leader. In Figure 10 we identify regions where $\hat{E}_n < 1$, meaning the follower flaps less than the leader and saves energy by flying behind it. We developed two strategies, greedy and cooperative, and we see that choosing the smallest flap for each follower independently is not only less efficient overall but also highly unstable. Hence, it is more beneficial to the population for a flyer to flap more than the greedy minimum and generate more wake for the follower behind it. It is also significantly more beneficial to fly in a formation than alone, with our model predicting a 24.3% reduction in the effort of the group.

References

[1] S. Ramananarivo, F. Fang, A. Oza, J. Zhang, and L. Ristroph, "Flow interactions lead to orderly formations of flapping wings in forward flight," *Physical Review Fluids*, vol. 1, no. 7, p. 071 201, 2016. DOI: 10.1103/PhysRevFluids.1.071201.

[2] C. Mavroyiakoumou, J. Wu, and L. Ristroph, "Modeling flying formations as flow-mediated matter," *arXiv preprint arXiv:2506.14025*, 2025.

[3] H. Weimerskirch, J. Martin, Y. Clerquin, P. Alexandre, and S. Jiraskova, "Energy saving in flight formation," *Nature*, vol. 413, no. 6857, pp. 697–698, 2001. DOI: 10.1038/35099670.

[4] H. Schlichting and K. Gersten, *Boundary-Layer Theory*, 9th. Springer, 2016.

[5] J. W. Newbolt, N. Lewis, M. Bleuët, J. Wu, C. Mavroyiakoumou, J. Zhang, and L. Ristroph, "Flow interactions between uncoordinated flapping swimmers give rise to group cohesion," *Proceedings of the National Academy of Sciences*, vol. 116, no. 7, pp. 2419–2424, 2019. DOI: 10.1073/pnas.1816098116.

[6] G. S. Triantafyllou, M. S. Triantafyllou, and M. A. Grosenbaugh, "Optimal thrust development in oscillating foils with application to fish propulsion," *Journal of Fluids and Structures*, vol. 7, no. 2, pp. 205–224, 1993. DOI: 10.1006/jfls.1993.1012.

[7] D. Floryan, T. Van Buren, C. W. Rowley, and A. J. Smits, "Scaling the propulsive performance of heaving and pitching foils," *Journal of Fluid Mechanics*, vol. 822, pp. 386–397, 2017. DOI: 10.1017/jfm.2017.302.

[8] J. Chico-Vázquez and C. Mavroyiakoumou, "Flapping strategies for flying formations," *arXiv preprint arXiv:2601.12920*, 2026.

Appendix

A Parameter Values

The dimensional and dimensionless parameters used throughout all simulations are listed in Tables 1 and 2.

Dimensional Parameters

Symbol	Value	Units	Description
ρ	1.0	$\mathrm{g\,cm^{-3}}$	Fluid density
μ	0.01	$\mathrm{g\,cm^{-1}\,s^{-1}}$	Dynamic viscosity
M	20	g	Flyer mass
c	3.8	cm	Chord length
s	8	cm	Span
A	10	cm	Flapping amplitude
f	1	Hz	Flapping frequency
C_T	1.0	—	Thrust coefficient
C_D	10.0	—	Drag coefficient
τ	0.5	s	Wake decay timescale

Table 1: *Physical parameters used in all simulations. The fluid properties ρ, μ, and chord c are from [1], as used in [2]. $C_T = 1$ is consistent with measurements in [6], [7]; $C_D = 10$ and $\tau = 0.5\,s$ are fitted and inferred from the same experimental data [1], [2].*

Dimensionless Parameters

Symbol	Value	Units	Description
γ	10	—	Combined thrust/drag parameter Equation (16)
χ	0.5	—	Dimensionless wake decay timescale Equation (17)

Table 2: *Dimensionless parameters used throughout all simulations. $\gamma = 10$ is fixed following [2]. $\chi = f\tau = 0.5$ is inferred from the experiments of [1].*

B Single Flyer

Figure 12 shows the single-flyer simulation. In **(a)**, we prescribe $V(t) = \pi A f \cos(2\pi f t)$ with $A = 10\,\text{cm}$ and $f = 1\,\text{Hz}$, hence an amplitude of $10\pi\,\text{cm}$. We then note that if the vertical velocity is positive, then the flyer is in the up-stroke, and if negative, then it is in the down-stroke. This is indicated on Figure 12 **(a)** and **(b)** with green and red shading respectively and in **(c)** with the colour of the trajectory.

In **(b)**, we see the forward velocity $U(t)$ as a result of the flapping. We can see that the flyer is moving horizontally forward the fastest in both the up- and down-strokes. This shows the symmetric nature of the current system.

Finally, in **(c)**, we plot the resultant path of the flyer in the horizontally co-moving frame $X - U^*t$, where U^* is the average forward velocity. The trajectory forms a symmetric figure-eight, reflecting the equal contributions of up- and down-strokes to the forward motion. An animation of the single-flyer simulation can be found here[10].

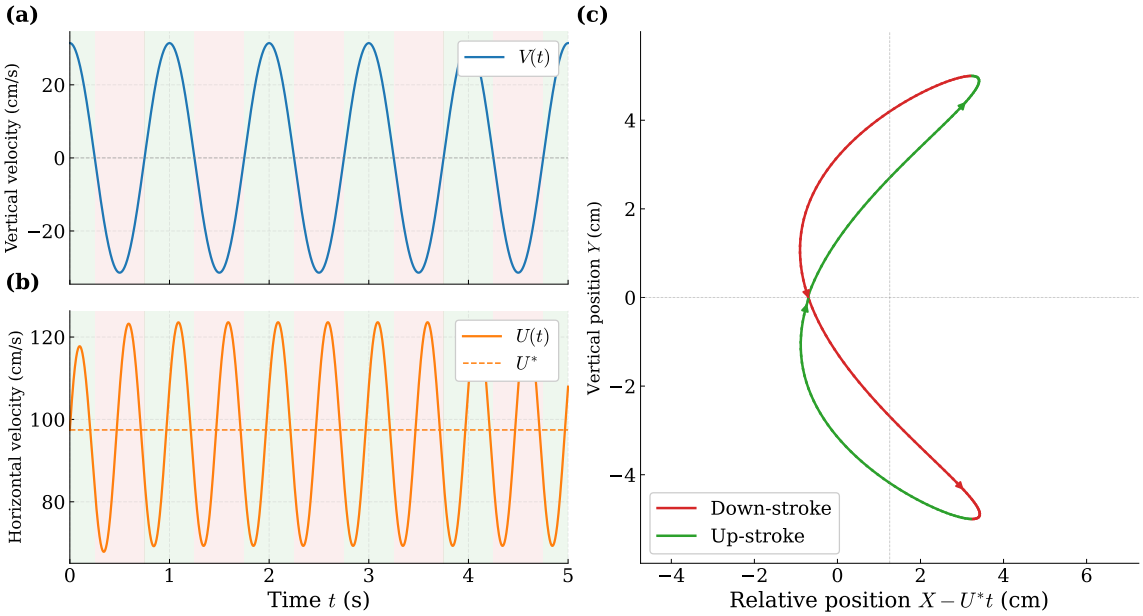


Figure 12: ***(a)*** *Flapping velocity $V(t)$; green/red bands mark up-/down-strokes.* ***(b)*** *Forward velocity $U(t)$ oscillating around the analytical U^* (dashed).* ***(c)*** *Resultant path in the co-moving frame — the symmetric figure-eight reflects equal up- and down-stroke contributions.*

[10] https://youtu.be/3KM2X9eWMZM

C Equilibrium Spacing

We derive the long-term average gap d^* between adjacent flyers following [2]. Assuming all flyers settle to the long-term average speed U^*, the gap $g_n = X_{n-1} - X_n$ is constant, $g_n = g^*$. Hence, the forces on the follower must vanish on average. Working in dimensionless variables, the follower's thrust term is proportional to B_n^2, where from Equations (1) and (4),

$$B_n(t) = \cos(2\pi t) - \cos(2\pi t_n)\, e^{-(t-t_n)/\tau}. \tag{32}$$

As we have constant separation in this long-term average sense, the delay between adjacent flyers passing through a given point is constant, say $\Delta t = g^*/U^*$. Now we can analytically express $t_n = t - n\Delta t = t - n\, g^*/U^*$. As our problem here is symmetric between sequential flyers, we look at the first pair. We define the dimensionless gap between the flyers to be $S^* = g^* f/U^*$, substituting into B_2,

$$B_2(t) = \cos(2\pi t) - \cos\big(2\pi(t - S^*)\big)\, e^{-S^*/(f\tau)}. \tag{33}$$

Integrating over a flapping period, the follower's mean thrust is

$$\langle B_2^2\rangle = \int_0^1 B_2^2\, dt = \tfrac{1}{2} + \tfrac{1}{2}e^{-2S^*/(f\tau)} - e^{-S^*/(f\tau)}\cos(2\pi S^*). \tag{34}$$

We set the leader's mean thrust to match the follower's, hence $\langle B_1^2\rangle = \langle B_2^2\rangle$. This simplifies to

$$\begin{aligned} \langle B_1^2\rangle &= \langle \cos^2(2\pi t)\rangle = \tfrac{1}{2} \quad \text{and} \\ \langle B_2^2\rangle &= \tfrac{1}{2} + \tfrac{1}{2}e^{-2S^*/(f\tau)} - e^{-S^*/(f\tau)}\cos(2\pi S^*). \end{aligned}$$

Hence,

$$\cos(2\pi S^*) = \tfrac{1}{2}\, e^{-S^*/(f\tau)}, \tag{35}$$

In the strong-interaction limit $f\tau \to \infty$, Equation (35) simplifies to $\cos(2\pi S^*) = 1/2$, giving the exact solutions $S^* = j + 1/6$ or $j + 5/6$ for $j \in \mathbb{N}$; the former are stable and the latter unstable [2]. For finite τ, we solve Equation (35) numerically for the first stable branch ($j = 1$), giving $S^* \approx 1.24$. With our parameter values ($A = 10\,\text{cm}$, $f = 1\,\text{Hz}$, $\tau = 0.5\,\text{s}$) this gives $U^* \approx 97\,\text{cm/s}$ and hence

$$d^* = S^*\lambda = S^*\frac{U^*}{f} \approx 1.24 \times 97 \approx 121\,\text{cm}. \tag{36}$$

This is the initial separation used in Section 6.

D Stability Diagram by Initial Gap

Figure 13 shows the stability outcome plots for each initial gap. Overlaying these on top of each other effectively gives Figure 7 in the main text, where if a point would have multiple outcomes, it is assigned as a mixed point.

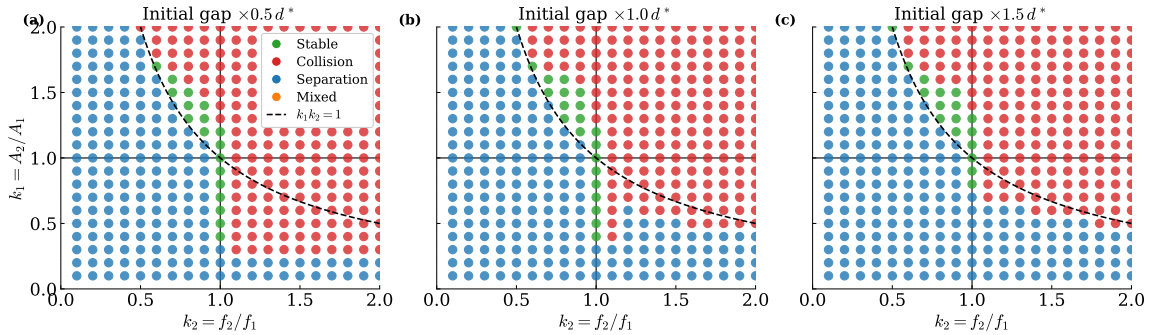


Figure 13: *Stability phase diagram broken down by initial gap.* ***(a)*** $0.5\,d^*$, ***(b)*** $1\,d^*$, ***(c)*** $1.5\,d^*$. *Green: stable. Red: collision. Blue: separation. The dashed curve is* $k_1k_2 = 1$.

E Optimal Effort Curves

Figures 14 and 15 show the full normalised effort curves $\hat{E}_n(d)$ for each follower under the greedy and cooperative strategies, for a three-bird formation with $d_{\min} = 0.3$. Without zooming in, these look very similar to each other, but if we look at d_2^* and d_3^* we see they do differ slightly.

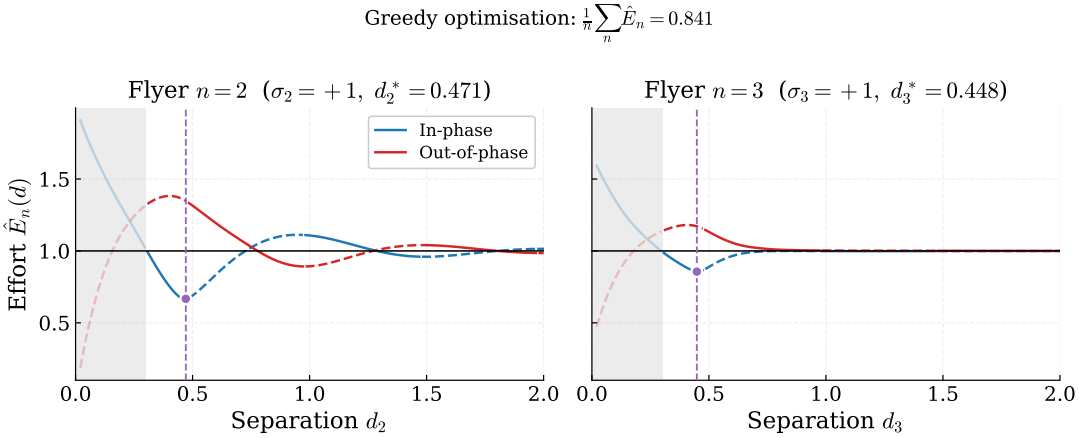


Figure 14: *Greedy optimisation effort curves for $N = 3$, $d_{\min} = 0.3$. Each panel shows $\hat{E}_n(d)$ with the in-phase (blue) and out-of-phase (red) choices. Solid segments are linearly stable, dashed unstable. The purple dot marks the greedy optimum d_n^* for each follower, chosen as the stable minimum of its own effort independently of the others.*

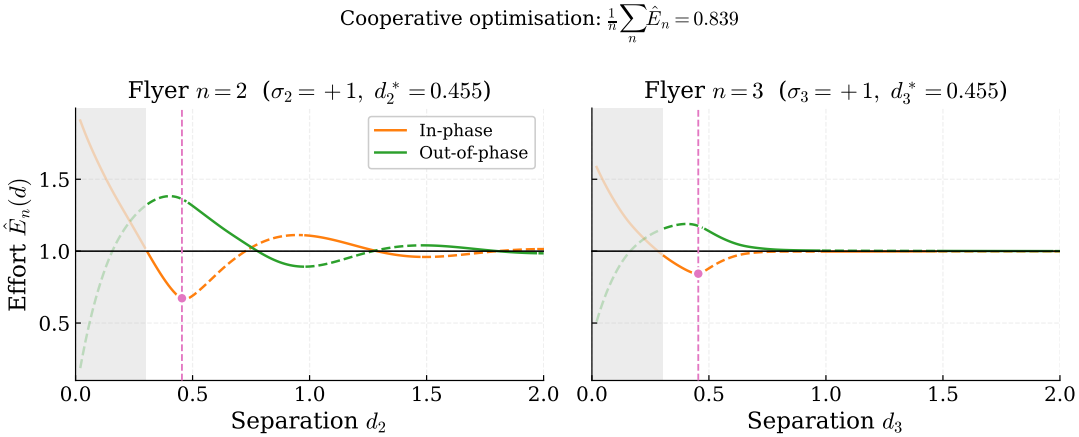


Figure 15: *Cooperative optimisation effort curves for $N = 3$, $d_{\min} = 0.3$. Each panel shows $\hat{E}_n(d)$ with the in-phase (orange) and out-of-phase (green) choices. The pink dot marks the cooperatively optimal d_n^*.*